Wavelength-Modulated Differential Photoacoustic (WM-DPA) imaging: a high dynamic range modality towards noninvasive diagnosis of cancer

Edem Dovlo*, Bahman Lashkari, Sung soo Sean Choi, Andreas Mandelis

Center for Advanced Diffusion-Wave Technologies (CADIFT), Department of Mechanical and Industrial Engineering, University of Toronto, Toronto, ON M5S 3G8, Canada

ABSTRACT

This study explores wavelength-modulated differential photoacoustic (WM-DPA) imaging for non-invasive early cancer detection via sensitive characterization of functional information such as hemoglobin oxygenation (sO_2) levels. Well-known benchmarks of tumor formation such as angiogenesis and hypoxia can be addressed this way. While most conventional photoacoustic imaging has almost entirely employed high-power pulsed lasers, frequency-domain photoacoustic radar (FD-PAR) has seen significant development as an alternative technique. It employs a continuous wave laser source intensity-modulated and driven by frequency-swept waveforms. WM-DPA imaging utilizes chirp modulated laser beams at two distinct wavelengths for which absorption differences between oxy- and deoxygenated hemoglobin are minimum (isosbestic point, 805 nm) and maximum (680 nm) to simultaneously generate two signals detected using a standard commercial array transducer as well as a single-element transducer that scans the sample. Signal processing is performed using Lab View and Matlab software developed in-house.

Minute changes in total hemoglobin concentration (tHb) and oxygenation levels are detectable using this method since background absorption is suppressed due to the out-of-phase modulation of the laser sources while the difference between the two signals is amplified, thus allowing pre-malignant tumors to become identifiable. By regulating the signal amplitude ratio and phase shift the system can be tuned to applications like cancer screening, sO_2 quantification and hypoxia monitoring in stroke patients. Experimental results presented demonstrate WM-DPA imaging of sheep blood phantoms in comparison to single-wavelength FD-PAR imaging. Future work includes the functional PA imaging of small animals *in vivo*.

Keywords: Differential Photoacoustic imaging, Wavelength modulation, Functional imaging, Frequency-domain, Cross-correlation, Biomedical imaging, Image improvement, Premalignant

1. INTRODUCTION

Biomedical photoacoustic (PA) imaging relies on the optical absorption properties of tissue to provide concentration maps of chromophores with remarkable contrast and spectroscopic-based specificity as well as spatial resolution due to its tissue-specific absorption of monochromatic light. It has therefore been investigated for early cancer diagnosis[1,2], particularly due to its sensitivity to blood oxygenation that enables potential measurement of critical diagnostic parameters for the metabolic state of lesions through enhanced laser light absorption in the tissue optical window (650-1100 nm). Using multiple wavelength optical sources makes molecular and spectroscopic imaging a possibility[3–6].

Cancer, known to be caused by genetic mutations, remains a major health problem worldwide causing one in 4 deaths in the United States[7] alone. It results in uncontrolled cell growth[8] raising nutrient and oxygen consumption compared to normal tissue[9], and therefore rapidly develops a dense microvasculature via angiogenesis to perpetuate tumor growth, and a drop in oxygenation levels within the tumor making it hypoxic. Assessing tumor hypoxia (a hallmark of cancer diagnostics) is a critical issue in cancer therapy management[10] and therefore of value to radiation oncologists, surgeons,

* edovlo@mie.utoronto.ca; phone 1-416-978-1287

Photons Plus Ultrasound: Imaging and Sensing 2016, edited by Alexander A. Oraevsky, Lihong V. Wang
Proc. of SPIE Vol. 9708, 97081Y · © 2016 SPIE · CCC code: 1605-7422/16/$18 · doi: 10.1117/12.2211761

and biotechnology and pharmaceutical companies involved in developing hypoxia-based treatment strategies to improve patient outcomes. Chances of survival increase considerably when detected and treated early[11].

There is a need for a suitable tumor hypoxia assessment modality for clinical applications. Among several measurement methods, existing noninvasive approaches that rely on endogenous markers and are thereby appropriate for *in vivo* clinical applications, include near-infrared (NIR) spectroscopy/tomography, blood oxygen level-dependent MRI (BOLD-MRI) and photoacoustic tomography (PAT)[6,12]. Limited tissue penetration and low spatial resolution[13] are however significant drawbacks for NIR spectroscopy whereas BOLD-MRI is prone to the influence of other independent variables not related to tissue oxygenation due to its is dependence on deoxyhemoglobin concentration[14] instead of pO_2 directly. Biomedical PAT detects less-scattering acoustic waves generated from absorbed electromagnetic energy with comparable axial resolution (~mm) and signal-to-noise ratio (SNR) facilitating accurate tumor hypoxia assessment[2].

1.1 Objective

This paper discusses a differential PA modality termed Wavelength-Modulated Differential Photoacoustic (WM-DPA) imaging that employs two laser wavelengths simultaneously to eliminate background noise by canceling out variations caused by the local fluence (capable of undermining spectral interpretation of PA images), thus yielding high sensitivity and specificity for accurate tissue hypoxia assessment.

Our frequency domain photoacoustic radar (FD-PAR) system uses chirp-modulated continuous-wave lasers, instead of the bulkier and expensive pulsed lasers used in conventional biomedical PA (time-resolved acoustic transient measurements[11,15]). The FD modality possesses depth-selective imaging capabilities[16] and applies matched filtering to generate high peak power cross-correlation response. The WM-DPA imaging system provides three images concurrently: separate images for the two applied wavelengths as well as the differential image. Further developments in image improvement techniques such as filtering and normalization are also investigated.

2. THEORY OF WM-DPA IMAGING

WM-DPA imaging employs chirp-modulated laser beams at two different wavelengths to generate PA signals from a chromophore. As shown in Figure 1, the first wavelength is selected so that the absorption difference between oxy- (HbO_2) and deoxy- (Hb) hemoglobin is minimum (i.e. at the isosbestic point of 805 nm) while the other such that the absorption difference is large (for instance, at 680 nm). The two chirps with identical sweep frequency, approximately have a π phase difference, which ideally causes the signal responses to cancel out each other at a specific (arbitrary) blood oxygenation level and thus, helps suppress background absorption and other noise, and amplify the difference between the two simultaneously generated signals. Minute changes in total hemoglobin concentration (tHb) and hemoglobin oxygenation (sO_2), which are useful in the determination of benchmarks of tumor formation such as angiogenesis and hypoxia, can be detected as a result.

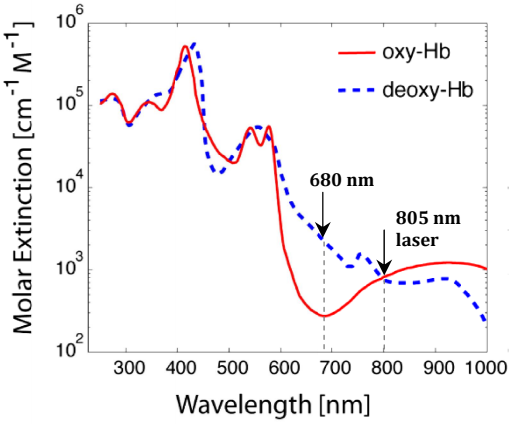

Figure 1: Molar extinction coefficient spectra for oxy- and deoxy- hemoglobin[17]

2.1 WM-DPA imaging of uniformly radiated long cylinder

For a small cylinder (axisymmetric model depicting the experimental samples), the pressure generated at the transducer location (equation (1)) as the laser beam spot size, $W \to \infty$ (i.e. large beam size) has been shown to approximate the 1D solution[18] as illustrated in Figure 2 assuming uniform irradiation using a Gaussian laser beam intensity profile, and ignoring the effect of absorption through the cylinder.

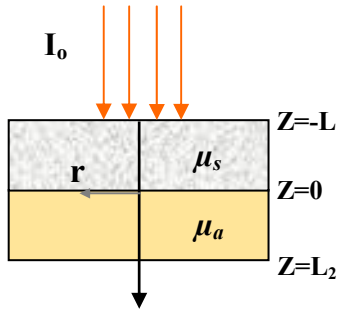

Figure 2: Simplified model of PA signal generation (1D model approximation)

$$\tilde{p}_s\left(z, r=0, f\right) \approx -j\omega\rho_s \frac{\beta_a \mu_a}{C_p}\left(\frac{j}{\mu_a + jk_a}\right)\left(\frac{1}{\rho_s k_a + \rho_a k_s}\right)\tilde{I}\left(\omega\right)e^{jk_s z} \qquad (1)$$

where the tilde indicates the Fourier transform; $\Gamma_a = \beta_a c_a^2 / C_p$ is the Grüneisen coefficient (efficiency of thermoacoustic excitation); β_a is the thermal expansion coefficient; C_p is the specific heat capacity; $k_a = \omega / c_a$ and $k_s = \omega / c_s$ are the absorbing and scattering media wavenumbers, respectively; c_a, c_s are the speed of sound in the absorbing and scattering media, respectively; $\omega = 2\pi f$ is the angular frequency; μ_a is the absorption coefficient in the absorbing medium (e.g. blood vessel, tumor); ρ_a, ρ_s are the densities of the absorbing and scattering media, respectively; r is the radial position; I is the laser intensity reaching the absorber.

In the FD modality, the delay time is determined by the cross-correlation of the output and linear frequency modulation (LFM) chirp input signals. The differential PA signal, and the cross-correlation function, can be obtained by summing the two respective detected PA signals from lasers A and B.

2.2 Hypoxia monitoring

Since the total hemoglobin concentration, c_{tHb} is the sum of c_{HbO_2} and c_{Hb}, and the oxygenation level, $sO_2 = c_{HbO_2} / c_{tHb}$, the absorption coefficient of hemoglobin for lasers A and B used in the WM-DPA modality can be described using Beer's law[2] as

$$\mu_a^{Hb}\left(\lambda_A\right) = \ln(10)\left[\varepsilon_{Hb}\left(\lambda_A\right)c_{tHb} + \left(\varepsilon_{HbO_2}\left(\lambda_A\right) - \varepsilon_{Hb}\left(\lambda_A\right)\right)sO_2 c_{tHb}\right] \qquad (2)$$

$$\mu_a^{Hb}\left(\lambda_B\right) = \ln(10)\varepsilon_{Hb}\left(\lambda_B\right)c_{tHb} \qquad (3)$$

where ε_{HbO_2}, ε_{Hb} are the extinction coefficients of HbO_2 and Hb, respectively; c_{HbO_2}, c_{Hb} are the concentrations of HbO_2 and Hb, respectively.

It should be noted that at the isosbestic point, i.e. $\lambda_B = 805nm$, the extinction coefficients of HbO_2 and Hb are equal causing the $\varepsilon_{HbO_2}\left(\lambda_A\right) - \varepsilon_{Hb}\left(\lambda_A\right)$ term to vanish, allowing c_{tHb} to be determined using equation (4) and furthermore, rearranging equation (3) to obtain sO_2. The detected differential PA signal is proportional to the difference in absorption coefficients at the specified wavelengths as

$$p_{AB} \propto \left(\mu_a^{Hb}(\lambda_A) - k\mu_a^{Hb}(\lambda_B)\right) = \ln(10)\begin{bmatrix}\left(\varepsilon_{Hb}(\lambda_A) - k\varepsilon_{Hb}(\lambda_B)\right)c_{tHb} \\ +\left(\varepsilon_{HbO_2}(\lambda_A) - \varepsilon_{Hb}(\lambda_A)\right)sO_2c_{tHb}\end{bmatrix} \quad (4)$$

where p_{AB} is the differential PA signal; k is an adjustable constant determined by the modulated amplitude ratio, $R = A_A/A_B$ and the phase difference, $dp = p_A - p_B$ of the two lasers. This is an important feature for such applications as cancer screening, identifying pre-malignant tumors, and hypoxia monitoring due to its high sensitivity to changes in optical blood parameters, particularly at suspected pre-malignant tumor regions, without exact parameter quantification.

3. EXPERIMENTAL SET-UP AND IMAGING PROCEDURES

The validity and sensitivity of the WM-DPA modality is tested in comparison to single-wavelength FD-PAR tomography by imaging plastic tubes (~2.67-mm inner diameter; 3.86-mm outer diameter) carrying heparinized sheep blood at various sO_2 levels. Detailed descriptions of the foundations of our WM-DPA (and FD-PAR) techniques are available elsewhere[6,19,20]. The photograph and block diagram of the experimental set-up are shown in Figure 3.

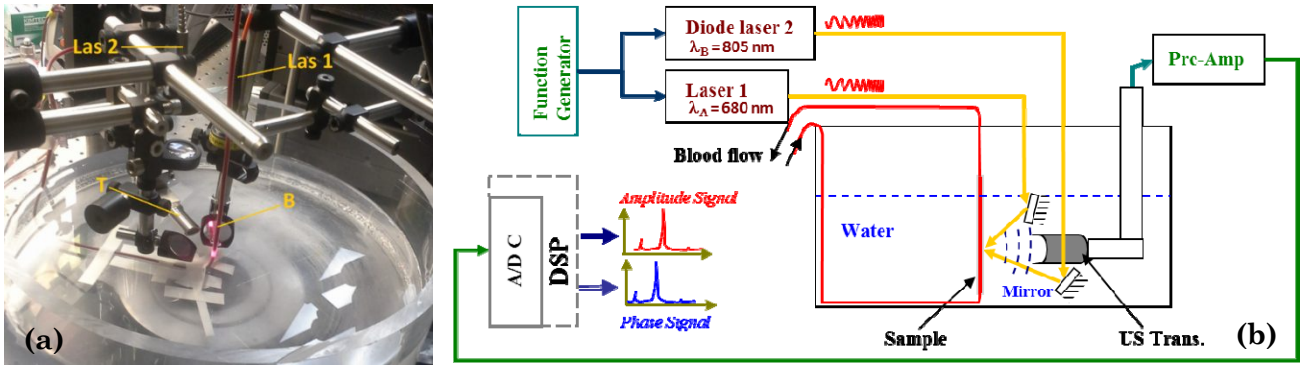

Figure 3: (a) Photograph, and (b) Block diagram of the experimental set-up of the WM-DPA system.
Las 1: Laser 1 (680 nm) fiber optic; Las 2: Laser 2 (805 nm) fiber optic; B: circulating blood (in tube); T: Single-element Transducer

A RPMC 680-nm (LDX-3230-680; MO, USA) laser and a Laser Light Solutions (LLS) 805-nm (LLS8800; Somerset, NJ, US) diode laser are employed for illumination in the experiment. The 680-nm laser, with a maximum optical power (out-of-fibre) of ~1.4W, is integrated with a customized laser driver (VFM5-25; MESSTEC, BY, DE) on an aluminum heat sink, while the 805-nm laser, with a maximum power of 15W, is modulated using a NI PXI-5442 (National Instrument, Austin, TX, USA) signal-generation card. A frequency-sweep range of 300 kHz–3 MHz is applied to the lasers. Both laser beams were collimated into 0.8-mm diameters via two collimators (F230SMA-B; ThorLabs, NJ, USA) and then directed to coincide at the same spot on the sample (with an acute incidence angle) by two protected silver mirrors with 25.4 mm diameter (PF10-03-P01; ThorLabs, NJ, USA). A convex lens placed in front of the 805-nm diode beam ensures an identical beam size for both lasers. A 3.5MHz single-element ultrasonic transducer (C383; Olympus Panametrics, CA, USA) that revolves around the sample is used to detect the PA signals generated. Most components of the set-up had freedom of motion in all directions (X, Y and Z). The sample and transducer were fully submerged in water for acoustic coupling, and the mirrors were also under water to minimize heat accumulation on the optics. A pre-amplifier (5662; Olympus Panametrics, CA, USA) was used for PA signal amplification. The NI PXIe-1065 ((National Instrument, Austin, TX, USA) data acquisition system collects the data needed for image reconstruction via signal processing using custom Lab View and Matlab software code.

The sample was placed at a distance of ~32-33 mm from the surface of the transducer, and 200 chirps were coherently averaged to enhance the SNR of the PA signals. Moreover, to optimize the WM-DPA method, the power of the two lasers was tuned to 1W (unity amplitude ratio; ~0.318 W/cm^2 power density over a 2-cm beam diameter) and the phase difference to 180^o so that the differential PA signal of HbO_2 was minimized. Sodium dithionite ($Na_2S_2O_4$) was mixed in with a small amount of the sheep blood and a small volume was repeatedly injected into the circulation tubing to deoxygenate the blood and obtain the various aforementioned oxygenation levels. The blood was allowed to circulate for

~10–15 min after each injection for uniform deoxygenation. A section of the blood-containing tubing was then imaged at every deoxygenation step. A gas analyzer (CCA-TS; OPTImedical, GA, USA) was used to measure blood parameters including sO_2 and tHb of the specific blood sample.

4. RESULTS AND DISCUSSION

Three sets of images were obtained for different blood oxygenation levels– 95.2% (I), 84.7% (II) and 73.0% (III). The images were first obtained without normalization or amplification. Upon normalization, the dynamic range for the differential PA image was observed to improve over the 680-nm (and significantly over the 805 nm) FD-PAR mode as shown in Figure 4 (and confirmed in Figure 5b). Each image is scaled to values within [0, 1] using the maximum amplitude in its respective column (680 nm, 805 nm and Differential). A common maximum was applied to the 680 nm and 805 nm images to facilitate adequate comparison (and portrayal of the sample). The absorber (blood at various sO_2 levels) is clearly observed at the same location consistently with a diameter of ~2.7 mm showing dimensional integrity with the tube dimensions. The maximum intensity of the image corresponds to the maximum signal amplitude obtained for a given mode, an indication of the presence of an absorber. The maximum image intensity at the ROI increases with decreasing sO_2 levels for the 680-nm wavelength, which validates the spectral trend of increasing absorption difference between HbO_2 and Hb at this wavelength. At the isosbestic point (805-nm), the maximum intensity at the ROI is similar for decreasing sO_2 levels, as expected. The differential PA mode was tuned to zero local fluence-induced variations at sO_2 level I, thereby resulting in enhanced sensitivity and specificity for accurate hypoxia monitoring (Figure 4). An increasing trend is thus observed for the differential PA mode for the decreasing sO_2 levels with improved dynamic range.

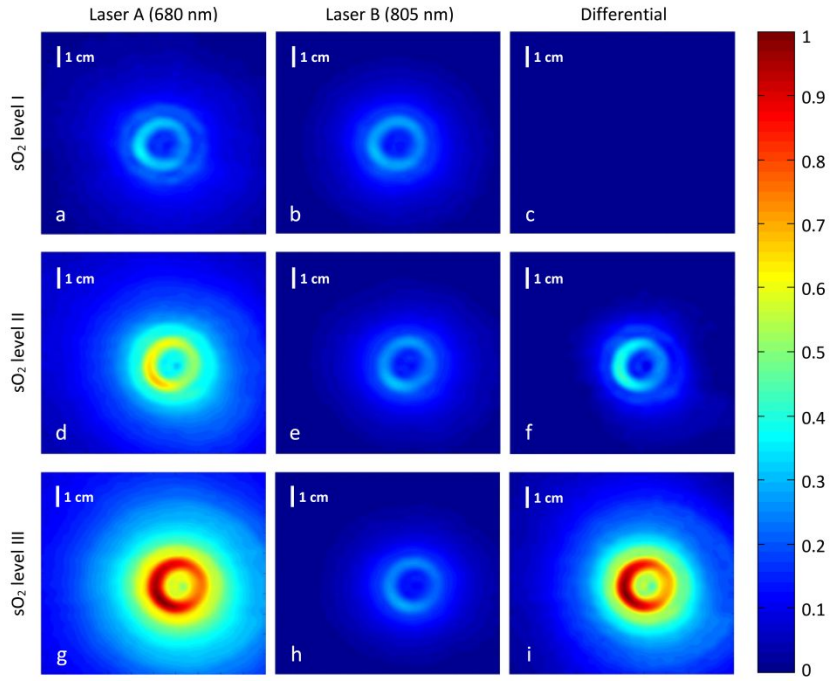

Figure 4: Normalized (column-wise) reconstructed PA image using the 680-nm laser only (a, d, g), PA image using the 805-nm laser only (b, e, h), and Differential PA image (c, f, i) using both lasers for circulating sheep blood in tube at sO_2 levels I (95.2%), II (84.7%) and III (below 73.0%)

Figure 5 clearly shows the significant improvement in the sensitivity and dynamic range of the WM-DPA system to changes in sO_2 levels and tHb. Background absorption and noise are highly suppressed (due to the out-of-phase modulation of the lasers) and the difference between the two PA signals is amplified. From the reconstructed images in Figure 4(c, f, i), it is seen that the WM-DPA method provides more resolved, better contrast and dimension-consistent images of the blood in the tube as the sO_2 level decreases compared to the 680-nm and 805-nm FD-PAR modes separately. The differential PA amplitude exhibited a 24.42% signal change per unit sO_2, demonstrating superior sensitivity compared to the single-wavelength FD-PAR measurements of 5.98% and 0.70% signal change per unit sO_2,

for the 680 nm and 805 nm modes, respectively. Optical fluence is significantly reduced as light travels towards the center of the tubing since it is strongly absorbed at the boundary of the blood and the tube. This is depicted, in particular, by the images of the deoxygenated blood (sO2 level III; Figure 4(g, h, i)) showing the high signal intensity ring at the boundary of the blood region and the tube diminishing with depth. The increasingly weaker signal surrounding the highly absorbing blood ring is likely a result of the spectral attenuation from the plastic tubing and the PA-generated US reflection off its surfaces. This is why it appears brighter/stronger with increased intensity of the generated PA signal (which is also reduced in the differential PA image compared to the 680 nm FD-PAR mode).

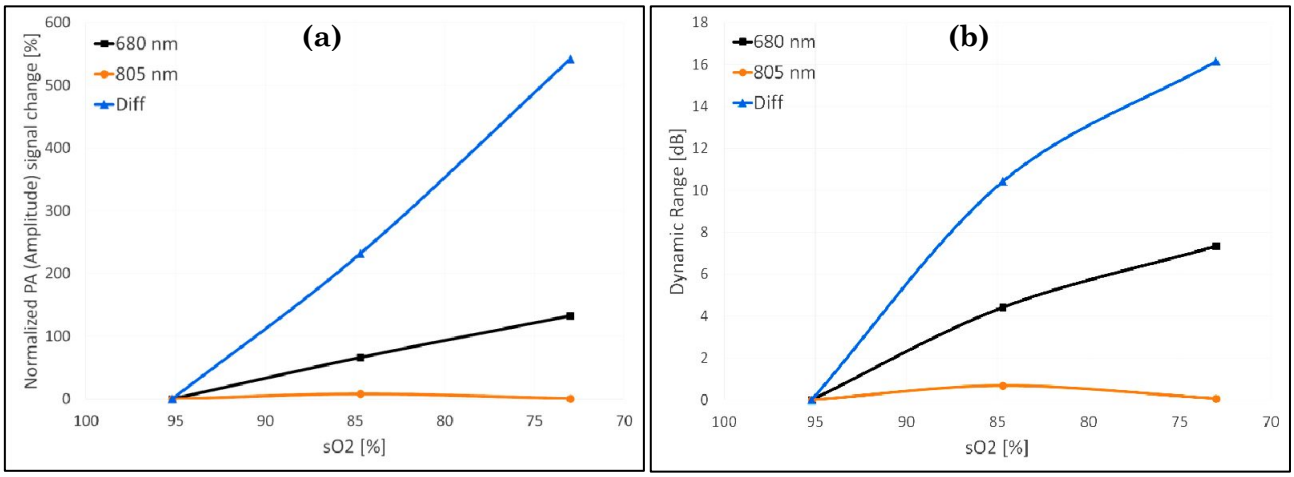

Figure 5: (a) Sensitivity and Dynamic range comparison of the tuned differential PA Amplitude signals with the corresponding single-wavelength FD-PAR signals

System optimization, particularly with respect to coupling the laser beams to be incident on the same spot on the sample and correcting for any delay time discrepancies between the two lasers are crucial in producing high quality images. A coupler will help better align the laser beams to the same spot. In addition to the single amplitude channel (also used in existing modalities), the WM-DPA mode can provide two complementary amplitude and phase channels which can further enhance the spatial resolution and SNR of images[19], and thus the reliability of hypoxia monitoring.

5. CONCLUSIONS

It was shown that the WM-DPA modality can be more sensitive to minute changes in tHb and sO_2, than single-wavelength FD-PAR imaging. This is valuable for clinical applications as benchmarks of tumor formation such as angiogenesis and hypoxia, can be detected. The feasibility of the method was demonstrated with experiments on heparinized sheep blood at decreasing oxygenation levels circulating in plastic tubing. Image normalization techniques were applied to improve WM-DPA imaging parameters such as dynamic range, SNR, contrast and spatial resolution. Future work includes the functional PA imaging of small animals *in vivo*.

ACKNOWLEDGEMENTS

AM is grateful to the Natural Sciences and Engineering Research Council of Canada (NSERC) for a Discovery Grant, and to the Canada Research Chairs Program.

REFERENCES

1. S. Mallidi, G. P. Luke, and S. Emelianov, "Photoacoustic imaging in cancer detection, diagnosis, and treatment guidance.," *Trends Biotechnol.* **29**(5), 213–221 (2011).
2. L. V. Wang and H. Wu, *Biomedical Optics: Principles and Imaging*, John Wiley & Sons (2012).
3. J.-T. Oh, M.-L. Li, H. F. Zhang, F. Hao, K. Maslov, G. Stoica, and L. V. Wang, "Three-dimensional imaging of skin melanoma in vivo by dual-wavelength photoacoustic microscopy.," *J. Biomed. Opt.* **11**(3), 34032 (2006).
4. D. Razansky, M. Distel, C. Vinegoni, R. Ma, N. Perrimon, R. W. Köster, and V. Ntziachristos, "Multispectral opto-acoustic tomography of deep-seated fluorescent proteins in vivo," *Nat. Photonics* **3**(7), 412–417, Nature

Publishing Group (2009).
5. S. Telenkov and A. Mandelis, "Signal-to-noise analysis of biomedical photoacoustic measurements in time and frequency domains.," *Rev. Sci. Instrum.* **81**(12), 124901 (2010).
6. B. Lashkari, S. S. Choi, E. Dovlo, S. Dhody, and A. Mandelis, "Frequency-domain Photoacoustic Phase Spectroscopy: A Fluence-independent Approach for Quantitative Probing of Hemoglobin Oxygen Saturation," *IEEE J. Sel. Top. Quantum Electron.* **PP**(99), 1–1 (2015).
7. R. Siegel, J. Ma, Z. Zou, and A. Jemal, "Cancer statistics, 2014.," *CA. Cancer J. Clin.* **64**(1), 9–29 (2014).
8. D. Hanahan and R. A. Weinberg, "The Hallmarks of Cancer," *Cell* **100**(1), 57–70 (2000).
9. P. Vaupel, F. Kallinowski, and P. Okunieff, "Blood flow, oxygen and nutrient supply, and metabolic microenvironment of human tumors: a review.," *Cancer Res.* **49**(23), 6449–6465 (1989).
10. P. P. Hsu and D. M. Sabatini, "Cancer cell metabolism: Warburg and beyond.," *Cell* **134**(5), 703–707 (2008).
11. M. Xu and L. V Wang, "Photoacoustic imaging in biomedicine," *Rev. Sci. Instrum.* **77**(4), 041101, AIP (2006).
12. G. F. Lungu, M.-L. Li, X. Xie, L. V. Wang, and G. Stoica, "In vivo imaging and characterization of hypoxia-induced neovascularization and tumor invasion.," *Int. J. Oncol.* **30**(1), 45–54 (2007).
13. M. Wolf, M. Ferrari, and V. Quaresima, "Progress of near-infrared spectroscopy and topography for brain and muscle clinical applications.," *J. Biomed. Opt.* **12**(6), 062104.
14. S. P. Li, A. R. Padhani, and A. Makris, "Dynamic contrast-enhanced magnetic resonance imaging and blood oxygenation level-dependent magnetic resonance imaging for the assessment of changes in tumor biology with treatment.," *J. Natl. Cancer Inst. Monogr.* **2011**(43), 103–107 (2011).
15. P. Beard, "Biomedical Photoacoustic Imaging: a review," *Interface Focus* **1**(4), 602–631 (2011).
16. S. a Telenkov and A. Mandelis, "Fourier-domain biophotoacoustic subsurface depth selective amplitude and phase imaging of turbid phantoms and biological tissue.," *J. Biomed. Opt.* **11**(4), 044006 (2006).
17. S. Prahl, "Optical Absorption of Hemoglobin," *Oregon Med. Laser Cent.*, 1999, <http://omlc.org/spectra/hemoglobin/> (accessed 13 January 2016).
18. B. Lashkari and A. Mandelis, "Linear frequency modulation photoacoustic radar: optimal bandwidth and signal-to-noise ratio for frequency-domain imaging of turbid media.," *J. Acoust. Soc. Am.* **130**(3), 1313–1324 (2011).
19. E. Dovlo, B. Lashkari, A. Mandelis, W. Shi, and F.-F. Liu, "Photoacoustic radar phase-filtered spatial resolution and co-registered ultrasound image enhancement for tumor detection.," *Biomed. Opt. Express* **6**(3), 1003–1009 (2015).
20. S. S. Choi, A. Mandelis, X. Guo, B. Lashkari, S. Kellnberger, and V. Ntziachristos, "Wavelength-Modulated Differential Photoacoustic Spectroscopy (WM-DPAS) for noninvasive early cancer detection and tissue hypoxia monitoring.," *J. Biophotonics* (2015).